Attenuation of Mouse Melanoma by A/C Magnetic Field after Delivery of Bi-Magnetic Nanoparticles by Neural Progenitor Cells

Raja Shekar Rachakatla,[†,∥] Sivasai Balivada,[†,∥] Gwi-Moon Seo,[†] Carl B. Myers,[⊥] Hongwang Wang,[‡] Thilani N. Samarakoon,[‡] Raj Dani,[‡] Marla Pyle,[†] Franklin O. Kroh,[§] Brandon Walker,[§] Xiaoxuan Leaym,[§] Olga B. Koper,[§] Viktor Chikan,[‡] Stefan H. Bossmann,[‡] Masaaki Tamura,[†] and Deryl L. Troyer[†,*]

[†]Department of Anatomy and Physiology, 228 Coles Hall and [‡]Department of Chemistry, 213 CBC Building, Kansas State University, Manhattan, Kansas 66506, United States, [§]NanoScale Corporation, 1310 Research Park Drive, Manhattan, Kansas 66502, United States, and [⊥]Department of Diagnostic Pathobiology, 223 Mosier Hall, Kansas State University, Manhattan, Kansas 66506, United States. [∥]These authors contributed equally to this work.

ABSTRACT Localized magnetic hyperthermia as a treatment modality for cancer has generated renewed interest, particularly if it can be targeted to the tumor site. We examined whether tumor-tropic neural progenitor cells (NPCs) could be utilized as cell delivery vehicles for achieving preferential accumulation of core/shell iron/iron oxide magnetic nanoparticles (MNPs) within a mouse model of melanoma. We developed aminosiloxane—porphyrin functionalized MNPs, evaluated cell viability and loading efficiency, and transplanted neural progenitor cells loaded with this cargo into mice with melanoma. NPCs were efficiently loaded with core/shell Fe/Fe_3O_4 MNPs with minimal cytotoxicity; the MNPs accumulated as aggregates in the cytosol. The NPCs loaded with MNPs could travel to subcutaneous melanomas, and after A/C (alternating current) magnetic field (AMF) exposure, the targeted delivery of MNPs by the cells resulted in a measurable regression of the tumors. The tumor attenuation was significant ($p < 0.05$) a short time (24 h) after the last of three AMF exposures.

KEYWORDS: nanotechnology · cell-based · targeted delivery · magnetic nanoparticles · magnetic hyperthermia · melanoma · neural progenitor cells

The incidence and mortality rate of malignant melanoma continues to increase at an alarming rate worldwide.[1] Disseminated melanoma is not curable using current clinical tools; traditional chemotherapy is ineffective due to inherent drug-resistant characteristics of the disease.[2,3]

The pioneering studies of Gordon *et al.* demonstrated induced intracellular hyperthermia using dextran magnetite nanoparticles in a high-frequency magnetic field (such as 500 kHz); the advantages of magnetic nanoparticles (MNPs), such as negligible or low toxicity, biocompatibility, injectability into the bloodstream, and potential accumulation in the target tumor, make them prime candidates for hyperthermia applications.[4] However, the specific absorption rates (SARs) of those early systems were low. It will be of great importance to achieve a high monodispersity of the magnetic nanoparticles because only then can the A/C excitation be optimized to achieve very high specific absorption rates. Magnetic hyperthermia has recently garnered new interest as a cancer therapy because technological advances allow heat delivery to be more precisely controlled and measured.[5] Hyperthermia (not necessarily magnetic hyperthermia) as an adjunct to radiotherapy or chemotherapy has been clinically tested for multiple human cancers, including recurrent malignant melanoma, lymph node metastasis, glioblastoma, cervical carcinoma, and head and neck squamous cell carcinoma.[6−8] Cancer cells were shown to be more sensitive to heat treatment than other cells.[9]

Despite its promise, magnetic hyperthermia of disseminated or deep tumors is currently complicated because it is difficult to target ferrofluid or magnetic nanoparticles to the tumor. To date, most reports of localized magnetic hyperthermia have described the direct tumor injection of milligram amounts of ferromagnetic materials. In some cases, limited success has been realized after antibodies or other ligands have been attached to MNPs.[10] However, further improvements in tumor targeting are needed.

Both direct killing effects and sensitization to other treatment modalities are dependent on distribution and duration of temperature elevation.[11] Bimagnetic particles (10−40 nm) are able to generate substantial heat within a magnetic field of low

*Address correspondence to troyer@vet.ksu.edu.

Received for review April 23, 2010 and accepted October 28, 2010.

Published online November 8, 2010.
10.1021/nn100870z

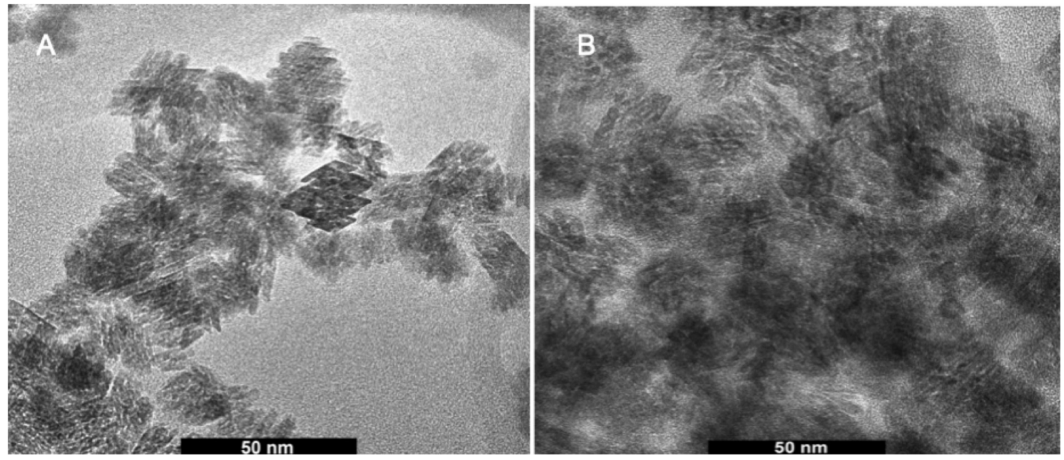

Figure 1. (A) TEM of Fe/Fe_3O_4 nanoparticles. (B) TEM of Fe/Fe_3O_4/ASOX/stealth nanoparticles.

strength and frequency.[12] The bimagnetic nanoparticles (MNPs) used here have a strong ferromagnetic iron core, which produces high temperatures with short AMF exposure,[13] a magnetic iron oxide shell for MRI,[14,15] an aminosiloxane-anchored oligoethylene glycol stealth coating, and chemically attached porphyrins (TCPP, tetra-4-carboxyphenyl porphyrin).

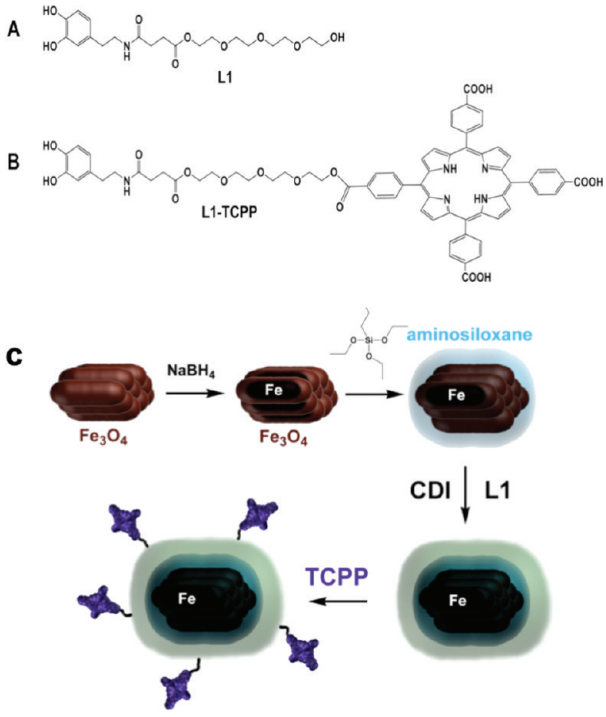

Scheme 1. (A) L1: basic dopamine-based stealth ligand. (B) L1-TCPP: targeting ligand for receptor-mediated cell uptake. TCPP is targeting the low density lipid (LDL) receptor. (C) Reaction sequence for the synthesis of TCPP-linked Fe/Fe_3O_4/ASOX/stealth nanoparticles: clusters of Fe_3O_4 nanorods are formed in reversed micelles upon addition of sodium borohydride. Further addition of $NaBH_4$ leads to the formation of iron(0) cores within the individual nanorods forming the clusters. The addition of 3-aminopropyltriethoxylsilane leads to the formation of aminosiloxane shells around the Fe/Fe_3O_4 nanoclusters. Addition of the organic stealth ligand L1 in the presence of CDI (carbonyl diimidazole) attached a dopamine-anchored organic stealth layer around the aminosiloxane layer. The final step consists of the addition of TCPP-targeting units to the Fe/Fe_3O_4/ASOX/stealth nanoparticles by reacting the terminal hydroxyl groups of the tetraethylene glycol units with one carboxylic acid group of TCPP (tetra(4-carboxyphenyl)porphyrin). EDC: 1-ethyl-3-(3-dimethylaminopropyl)carbodiimide. HOBT: 1-hydroxybenzotriazole.

Our prior work revealed attenuation of melanomas after AMF treatment when microgram amounts of MNPs (with attached porphyrins) was given intravenously.[16] Many proteins have been found to be instrumental in the progression of melanoma.[17−19] Two-dimensional gel electrophoresis followed by MALDI-TOF MS (matrix-assisted laser desorption/ionization-time-of-flight mass spectrometry) is a powerful proteomic approach as exemplified by its use in 2009 to find differentially expressed proteins in pancreatic cancer tissue.[20] This approach has been used to identify proteins highly over- or under-expressed in other cancerous *versus* normal tissues.[20−22] Here, we used this approach to investigate protein expression after localized AMF treatment.

Many attempts have been made to increase localization of various kinds of nanoparticles, including magnetic nanoparticles for imaging or therapy, to tumors. For example, particles have been tagged with antibodies recognizing tumor-specific epitopes[23,24] or peptides binding to receptors on tumor cells or neovasculature.[25−27] Tumor-homing cells have been used as delivery vehicles for targeted gene therapy for preclinical models of cancer.[28−32] In addition to being used to deliver genes, bone marrow stem cells have been loaded with iron oxide nanoparticles and used to target murine lung cancer for MRI.[33] Here, we report for the first time the utilization of neural progenitor cells (NPCs) as a sort of "Trojan horse" to target core/shell MNPs to preclinical melanoma, with subsequent tumor reduction after exposure to an A/C magnetic field. There are several potential advantages inherent in this paradigm beyond superior targeting. First, the MNP cargo within the cells is hidden from the reticuloendothelial system. Second, the tumor-tropic cells themselves could be engineered to secrete proteins, such

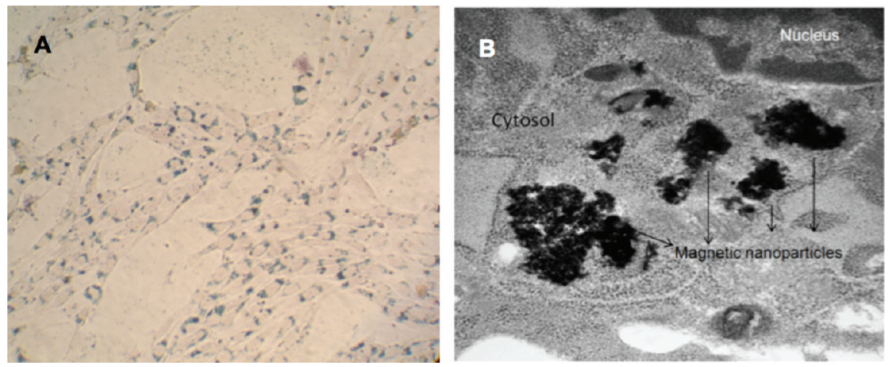

Figure 2. (A) Bright-field image of NPCs loaded with MNPs showing positive Prussian blue staining for the presence of iron and counterstained with nuclear fast red (magnification 20×). (B) Transmission electron microscopy image of NPC loaded with MNPs (magnification 30 000×).

as cytokines, to enhance the effect of regional hyperthermia. Third, the homing cells could also potentially carry other chemical payloads into the tumor. In this way, both the MNPs and adjunct therapy could be targeted to the tumor simultaneously.

RESULTS AND DISCUSSION

Nanoparticles. The nanoparticle synthesis is depicted in Figure 1 and Scheme 1. Nanoparticle characteristics are detailed in the Materials and Methods section.

Loading Studies of MNPs on NPCs. MNPs efficiently loaded into NPCs. After Prussian blue staining, MNPs were detected in NPCs as blue staining material (Figure 2A). Electron microscope images of NPCs showed loaded MNPs as aggregates in the cell cytoplasm (Figure 2B). Close examination of additional TEM images revealed that in some images the aggregates were surrounded by fragmented unit membrane, indicating they were possibly in an endosomal compartment (Figure S1, Supporting Information). In most images, they did not appear to be so enclosed. On the basis of these results, we believe that the MNPs are taken up *via* the LDL receptor and traffic in the endosomal−lysosomal system but cause endosomolysis with subsequent release of MNPs into the cytosol. Interestingly, the high-resolution transmission electron microscopy (HRTEM) images (Figure 1) of the MNPs show them as nanorod-like structures forming clusters, which in turn appear to be associated with each other. However, HRTEM is carried out in high vacuum in which the oligoethylene glycols tend to strongly adhere to one another. The loading efficiency of MNPs into NPCs increased with increasing concentration of MNPs in medium. The highest concentration of 5 pg of iron per cell was identified in cells incubated with medium containing 25 μg/mL iron (Figure 3).

Cytotoxicity of MNPs on Neural Progenitor Cells and B16-F10 Cells. MNP toxicity was tested based on iron concentration in MNPs. Media containing various iron concentrations of MNPs were added to NPCs and B16-F10 cells and incubated overnight. The toxic effect of these MNPs increased with increasing iron concentration. Cell viability assessment for varying concentrations of MNPs on NPCs and B16-F10 cancer cells is shown in Figures 4 and 5, respectively. NPCs tolerated the MNPs well through 20 μg/mL iron concentration (Figure 4), so this MNP concentration was used for subsequent experiments. However, the B16-F10 cell number was decreased upon exposure to only 10 μg/mL iron concentration (Figure 5).

There are several possible reasons the mouse melanoma cells are more vulnerable to the MNPs than the neural progenitor cells used in this study. One plausible explanation could be that, since the interior of the cancer cells is more basic than most normal cells,[34] biocorrosive damage to the aminosiloxane shell of the MNPs could expeditite cytotoxicity due to increased oxidative stress. Second, since the potentially toxic cetyl trimethylammonium bromide (CTAB) surfactant is located on the interior of the silica shell, more of it could be released in the relatively more alkaline environment in the interior of the cancer cell compared to a normal cell. The increased cytotoxicity to B16-F10 cells does not ap-

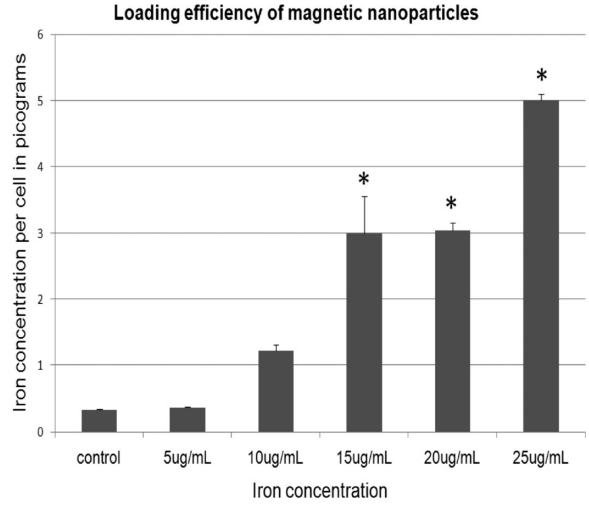

Figure 3. Loading efficiency of iron MNPs: iron concentration per NPC cell loaded with various concentrations of MNPs. * Statistically significant ($p < 0.05$) when compared with the control. The fact that uptake increases rapidly at 15 μg/mL but then remains stable at 20 μg/mL most probably reflects the fact that, for unknown reasons, there was more variation in the 15 mg/mL group (as reflected by SE) than other groups.

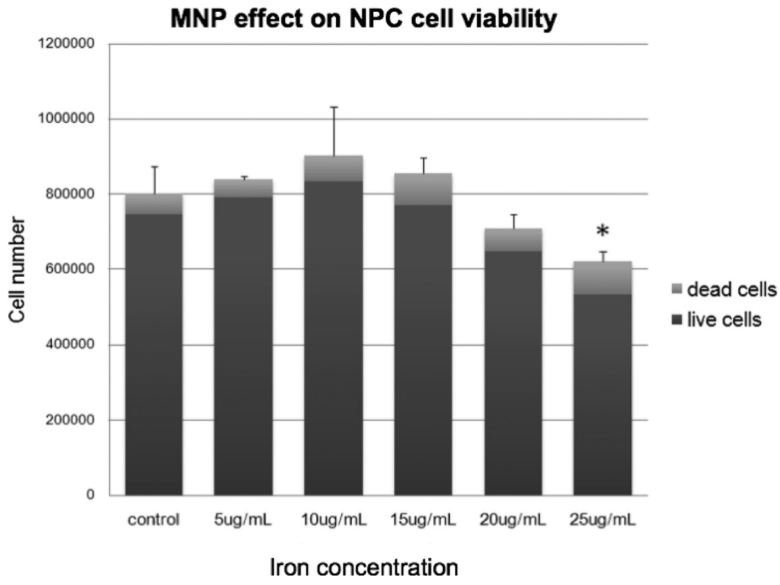

Figure 4. *In vitro* cell viability of NPCs cultured in medium containing increasing concentrations of iron MNPs. * Statistically significant ($p < 0.05$) when compared with the control.

pear to be due to increased MNP uptake; uptake levels are similar to those in NPCs (data not shown).

AMF-Induced Temperature Changes *In Vitro*. It was not possible to insert the optical probe into the melanomas because when this was attempted there was leakage of the gelatinous tumor parenchyma from the entry wound created by the probe. Hence, we mimicked the tumor environment by overlaying agarose onto pelleted NPCs loaded with MNPs or NPCs alone; the agarose was then allowed to gel in a microcentrifuge tube. Temperature increase over time was compared between NPC controls and MNP-loaded NPCs (NPC-MNP) (Figure 6). When we measured the temperatures at the pellet, there was a significant 2.6 °C increase between control and MNP-loaded cells ($p < 0.1$) after 10 min AMF exposure time. When we measured temperatures farther from the pellet, in the middle of the agarose, there was a small temperature increase in both the groups due to residual heating; during AMF exposure, the induction coil heats slightly and transfers its heat to the tube through air.

NPC-MNP and A/C Magnetic Field Effect on Melanoma. NPCs have tumor-tropic properties, and many groups have successfully used NPCs as therapeutic delivery vehicles to tumors.[29,35,36] Substantial numbers of MNP-loaded NPCs were identified in tumor sections 4 days after IV administration (Figure 7D). On the basis of reports in the literature, which have estimated 20−40% of transplanted stem cells homed to tumors in rodents,[37,38] we assume that about 20% of the administered cells migrated to the tumors. Other stem cells shown to home effectively to tumors include bone marrow stem cells[39] and adipose-derived mesenchymal stem cells.[40] We have previously shown that umbilical cord matrix stem cells can efficiently be used for cell-based gene therapy in a preclinical model for human breast cancer.[41−43]

To test the hypothesis that administration of NPCs loaded with MNPs followed by AMF application would reduce the tumor burden, NPC-MNPs were injected intravenously into melanoma-bearing mice. Tumor volume comparisons are graphed in Figure 8. The smallest tumor volumes were observed in the group receiving NPCs loaded with MNPs+AMF; the difference in tumor volume when compared with the saline group was significant at day 12 post-tumor cell inoculation. We did not find any significant difference between tumor-bearing mice receiving NPC-MNP but no AMF and the saline group. There was tumor seepage after day 12 in the saline group due to the increase in tumor sizes; hence, the tumor volume measurements were not taken after day 12. After 15 days, all of the mice were euthanized and tissues were collected for further histochemical studies.

We did not find MNP-NPCs in tumor tissues from mice subjected to AMF exposure and evaluated at the end of the experiment (Figure 7C). This absence may indicate that the NPCs perished and released their cargo,

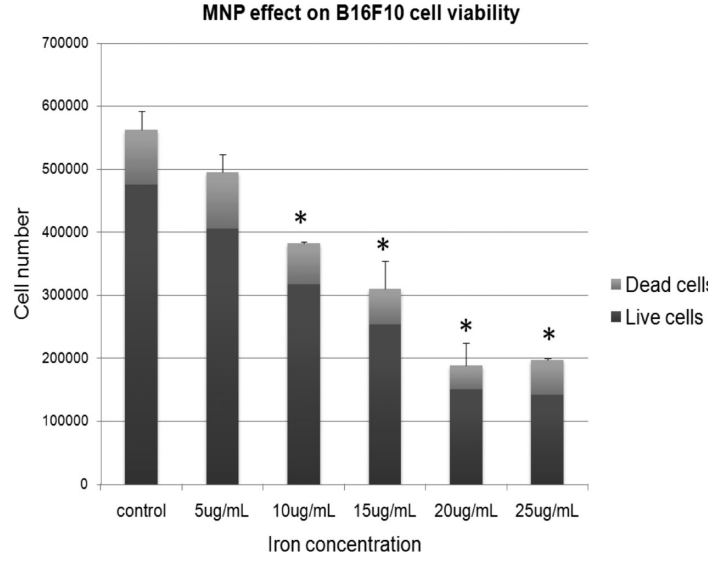

Figure 5. *In vitro* cell viability of B16-F10s cultured in medium containing increasing concentrations of iron MNPs. * Statistically significant ($p < 0.05$) when compared with the control.

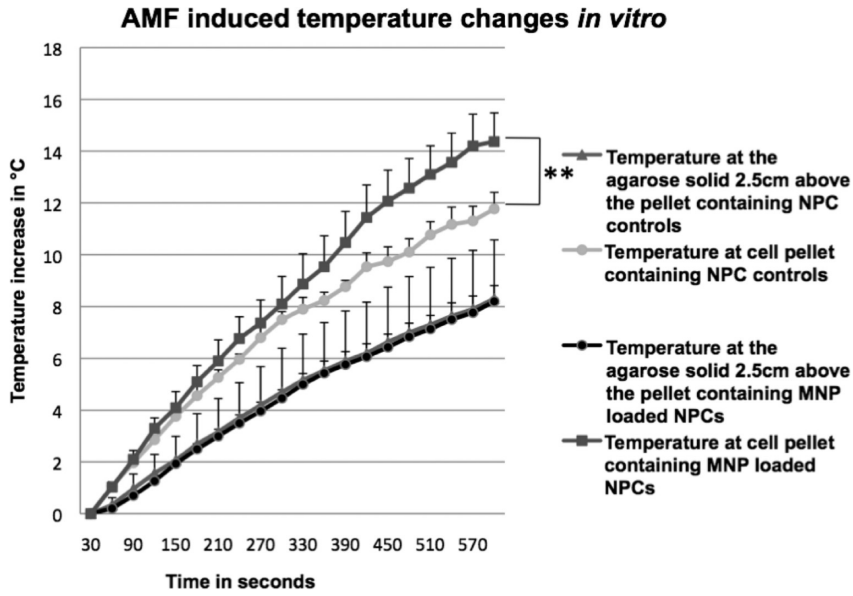

Figure 6. AMF-induced temperature changes *in vitro*. Temperature measurements after AMF of NPCs loaded with MNPs and NPC controls at the pellet and in the agarose solid. ** Statistically significant ($p < 0.1$) when compared with the control.

which was subsequently removed from the site by phagocytic cells.

The MNP-loaded NPCs themselves without A/C magnetic field exposure had a measurable but insignificant tumor inhibition effect. We observed a similar effect in previous work testing the MNPs alone.[16] It is our hypothesis that this effect could be due to biocorrosion of the MNPs with subsequent release of iron (II/III), resulting in oxidative damage to tumor tissue.[44] Furthermore, we have shown that traces of surfactants that have been used for the synthesis of the iron/iron oxide nanoparticles from reverse micelles (especially CTAB) become incorporated during synthesis of the MNPs and are released during the process of biocorrosion.[45] It is obviously an advantage with the stem-cell-based approach that the effects from biocorrosion and surfactant release stay hidden within the delivering stem cells until they traffic to the tumor. Therefore, they will cause minimal damage elsewhere but will augment the hyperthermia effect in the tumors.

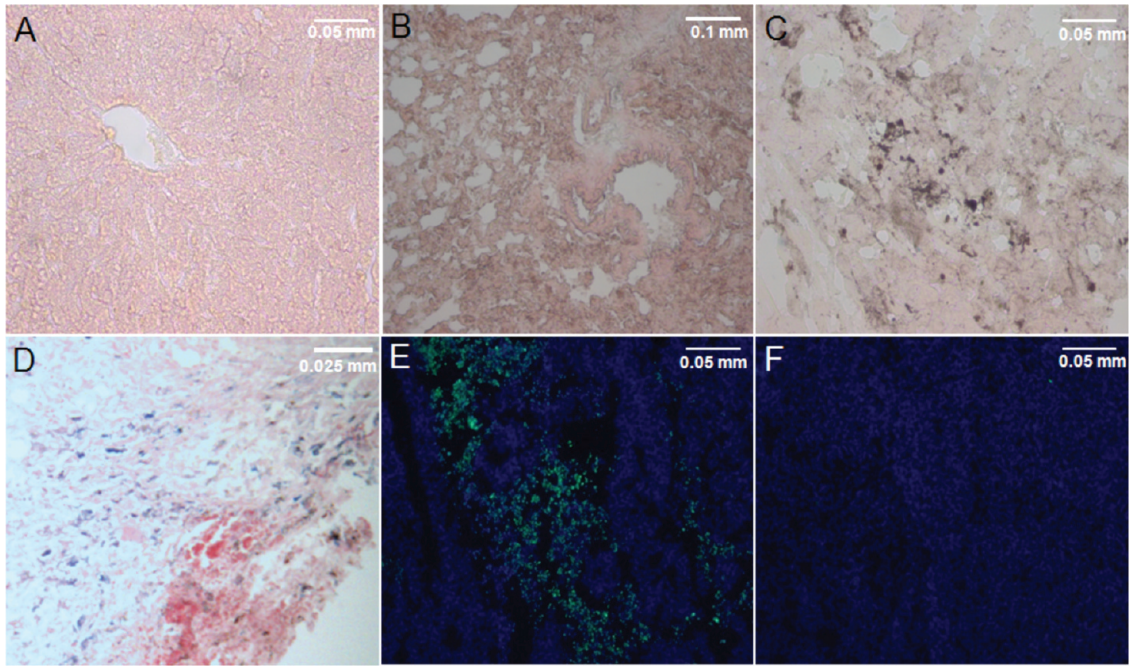

Figure 7. (A–D) Prussian blue stained tissue sections, counterstained with nuclear fast red, of melanoma tumor-bearing mice which received NPC-MNP followed by AMF treatment: lung (A), liver (B), and tumor (C); note the absence of blue stained NPCs in the tumor sections. Positive Prussian blue stained NPCs loaded with MNP in tumor section of a mouse which received NPC-MNP but no AMF treatment (D). (E,F) TUNEL assay: green apoptotic cells in a tumor-bearing mouse with NPC-MNP+AMF (E) compared to few apoptotic cells in a tumor-bearing mouse with saline only treatment (F).

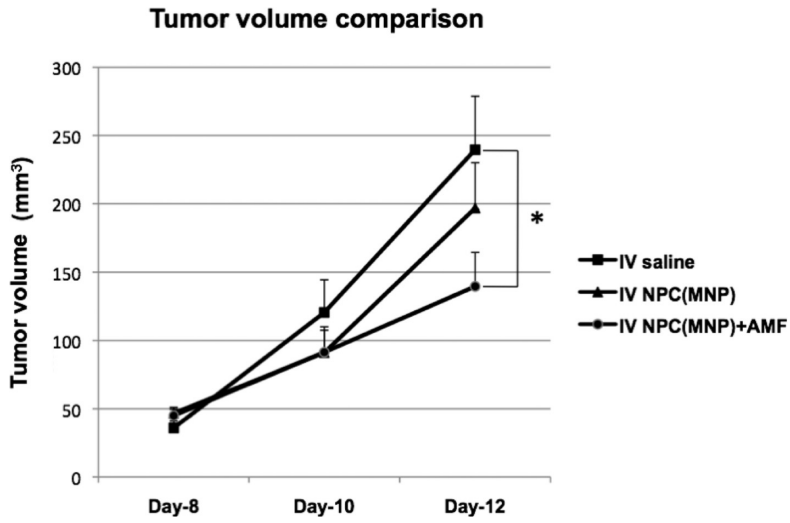

Figure 8. Tumor volumes in mice injected with B16-F10 melanoma cells. Mice injected with saline compared to mice injected with NPC-MNP with or without AMF treatment. * Statistically significant ($p < 0.05$) when compared with saline control.

To our knowledge, this is the first report showing that tumor-tropic stem cells loaded with MNPs *ex vivo* and administered intravenously can result in regression of preclinical tumors after A/C magnetic field exposure. Ikehara *et al.* injected oligomannose-coated liposomes encapsulating Fe_3O_4 and 5-fluorouracil (5-FU) into the peritoneal cavity with subsequent uptake by peritoneal macrophages and delivery to peritoneal gastric tumors in a mouse model. After AMF exposure, they observed significant attenuation of the peritoneal tumors.[46] The localized hyperthermia caused release of the 5-FU from the macrophages. We recently evaluated porphyrin functionalized core/shell Fe/Fe_3O_4 MNPs similar to the ones used here for localized hyperthermia but not administered in cells.[16] In that report, we showed that even microgram amounts of the MNPs given intratumorally or intravenously could reduce subcutaneous melanomas. However, Prussian blue staining for iron was much more pronounced in the lungs and liver than in the work reported here. Thus, an advantage of the cell-based delivery of the MNPs seems to be that it avoids agglomeration in the reticuloendothelial (mononuclear phagocytic) system.

Although the probable accumulation of MNPs reported here is low compared to most reported tumor accumulations *in vivo*, the iron core of the MNPs used in this work may allow smaller amounts of the MNPs to respond to an A/C magnetic field *in vivo* than would be expected for iron oxide MNPs. Iron oxides show distinctly smaller mass magnetizations ($\mu_s = 60-100$ Am^2 kg^{-1}, per weight unit of magnetite) and coercivities, which typically range from 8000 to 16 000 Am^{-1} compared to iron.[47] In contrast, for Fe(0) nanoparticles featuring a diameter below 8 nm, which are usually superparamagnetic, the mass magnetization is approximately $\mu_s = 100$ Am^2 kg^{-1} with intrinsic coercivity less than 1000 Am^{-1}.[48,49]

It is noteworthy that heating of the whole tumor region by using relatively large amounts of Fe/Fe_3O_4/aminosiloxane (Fe/Fe_3O_4/ASOX) nanoparticles may be unnecessary. Because of the very small iron(0) cores in the Fe/Fe_3O_4 clusters consisting of several nanorods (5−10 nm in length, 1−4 nm in diameter), A/C magnetic heating should mainly occur according to the Neel mechanism,[49] resulting in the local heating of the nanoparticles. Larger nanoparticles ($d > 20$ nm) feature the Brownian mechanism of heating, resulting in a much better stirring at the nanoscale level. The presence of the tetraethylene glycol units leads to a tight binding of water molecules to the nanoparticles, which may further decrease the local diffusion. Therefore, "hot spots" featuring a temperature above 45 °C may exist during A/C magnetic heating, which can lead to local damage of the cells at multiple locations, even when the total temperature of the tumor tissue is not significantly enhanced.

It is probable that tumor attenuation is improved by other factors in addition to A/C magnetic field exposure after MNP delivery to tumor by NPCs. Cytokines released by the NPC-MNP after hyperthermia may enhance the attenuation; a recent report indicates that conditioned medium from heat-treated mesenchymal stem cells significantly inhibited proliferation of cancer cells *in vitro*.[50,51] Another factor that could enhance the antitumor effect of mild to moderate regional hyperthermia *in vivo* is stimulation of the innate immune response. Recently, for example, it has been shown that elevating local tumor temperature to only 41−43 °C is sufficient to activate natural killer (NK) cells.[52] NK cells are part of the innate immune system and are potent tumor-lytic agents when activated.[53] Kubes *et al.* showed that high numbers of activated monocytes with increased cytotoxic effector function were recruited into B16-F10 melanoma-bearing mice after mild local microwave hyperthermia.[54]

We collected tumors 24 h after the last AMF treatment on some of the mice to investigate potential mechanisms of attenuation. We found that the apoptotic index was increased in the NPC-MNP IV transplanted group after three rounds of AMF, indicating that the targeted magnetic hyperthermia had a measurable effect on cell viability 24 h after the last treatment (Figure 7E). This corresponds to the time at which subcutaneous tumor volumes in the group receiving NPCs loaded with MNPs and subsequent AMF were significantly less than tumor volumes in any of the other

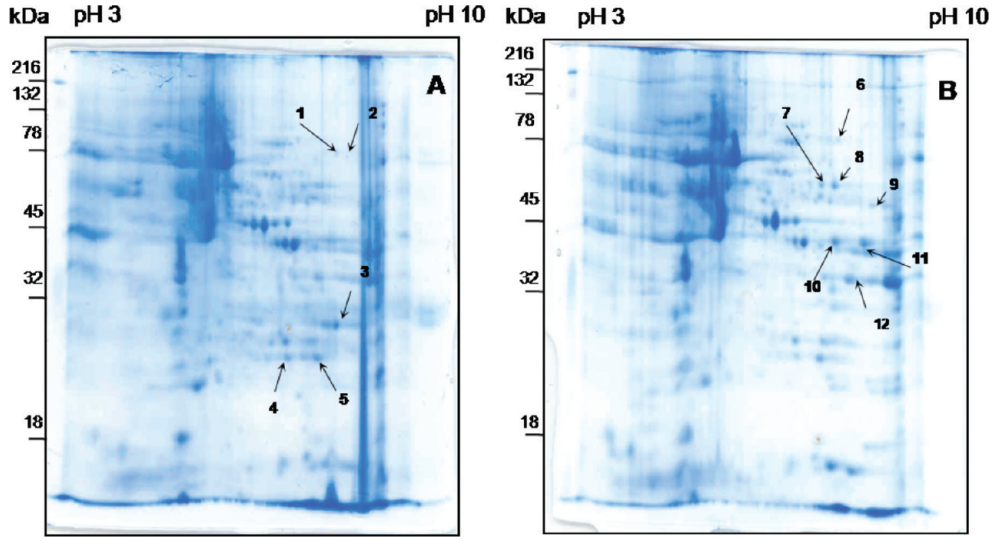

Figure 9. Two-dimensional gels of melanoma tissues from mice treated with saline+AMF or NPC-MNP+AMF. Tumor samples from mice receiving saline+AMF (A) and NPC-MNP+AMF (B) were harvested and processed for 2-D electrophoretic separation. The protein samples were focused using 3-10 linear IPG strips for the first dimension, electrophoretically separated on 12% acrylamide gels, and stained with Biosafe Coomassie G-250. Numbers with arrowhead lines refer to protein spots identified by MALDI-TOF analysis.

groups. Hence, apoptosis appears to be a mechanism involved in reduced tumor volumes.

Proteomic Analysis. To further investigate the mechanisms by which our treatment attenuates melanoma, we examined the effect of our treatment on differential expression of proteins by the melanoma cells. Tumors were excised from mice receiving either NPC-MNP followed by AMF or saline followed by AMF. Total protein was extracted from these tumors, and the extracted proteins were separated using 2-D gel electrophoresis. Gel spots representing 12 proteins expressed differentially in the 2 mouse groups were pinpointed using the MASCOT identification search software for identifying peptide mass fingerprinting (PMF). These protein spots are noted in Figure 9. We attempted to identify each of the proteins comprising the 12 differentially expressed spots using MALDI-TOF mass spectrometry. Identified proteins are listed in Table 1. As can be seen, phosphoglycerate kinase 1 (PGK1) and neurotensin receptor 1 protein were much more highly expressed in tumors from the mice receiving intravenous NPC-MNP followed by AMF treatment than in the saline+AMF controls. The group receiving NPCs+ AMF alone was not included in this comparison because Prussian blue staining failed to identify any intact NPCs in NPC-MNP treated tumor tissue at the end of the experiment, indi-

TABLE 1. Proteins of Melanoma Tumor Treated with Saline+AMF and NPC-MNP+AMF, Analyzed by MALDI-TOF[a]

proteins of AMF[b] exposed NPC-MNP[c] injected tumor and saline injected tumor were analyzed by MALDI-TOF					
spot number	protein identification	GenBank numbers	theoretical MW (Da)	pI	sequence coverage (%)
saline+AMF					
1	TNF receptor-associated factor 6	gi6755867	65679	7.71	14
2	Aste 1 protein	gi68534685	69927	8.31	12
3	β-globin	gi156257677	15823	7.14	78
4	biliverdin reductase B	gi21450325	22299	6.49	53
5	unnamed protein product	gi74222020	27054	6.90	39
NPC-MNP+AMF					
6	Zmym1 protein	gi116283425	103513	8.88	10
7	neurotensin receptor 1	gi9055296	47708	9.39	19
8	unnamed protein product	gi74211198	54416	10.00	13
9	unnamed protein product	gi74211198	51420	9.09	16
10	phosphoglycerate kinase 1	gi70778976	44928	8.02	43
11	phosphoglycerate kinase 1	gi70778976	44928	8.02	53
12	similar to glyceraldehyde-3-phosphate dehydrogenase	gi149252413	34190	8.45	27

[a]Spot numbers refer to the regions in the resolved proteins (as shown in Figure 9) picked for MALDI-TOF analysis. Spots with different numbers but the same protein identification (*e.g.*, spots 10 and 11) most likely represent two forms of the same protein which have different post-transcriptional or post-translational modifications. [b]AFM: alternating magnetic field. [c]NPC-MNP: neural progenitor cells loaded with magnetic nanoparticle.

cating that the NPCs had been killed at some point by the A/C magnetic field exposure. Thus, it is unlikely that any differences in protein levels are due to the presence of the delivery cells. Also, it is unlikely that the NPCs, which are a minor population, could secrete enough protein to register as a difference to be picked as spots on the second dimension gels even had they survived.

Of the seven protein spots found in the treated group but not the saline group (replicated four times; see Table 1), one candidate protein identified that could potentially exert an antitumor effect is PGK1, which is antiangiogenic when overexpressed in some tumors.[55] However, overexpression of PGK1 in prostate cancer has been shown to facilitate tumor growth.[56] On the other hand, there were five protein spots present in the saline control group that were not present in the treated group. One of these was TNF receptor-associated factor 5 (TRAF5), which is known to activate NF-κB.[57] Another, biliverdin reductase B, also increases NF-κB expression.[58] NF-κB is a central player in the transition to a more invasive state in many tumors.[59] Biliverdin reductase B was identified as a specific protein marker in microdissected hepatocellular carcinoma,[60] elevated in methotrexate-resistant colon cancer cells,[61] and is induced in renal carcinoma.[62] Hence, it possible that down-regulation of these genes could have been a factor in reduction of tumor size. While preliminary, these findings provide the background for further investigation to reveal potential mechanisms of tumor attenuation by AMF after targeted delivery of MNPs by tumor-tropic stem cells.

CONCLUSIONS

In conclusion, we show here that (1) NPCs efficiently load with core/shell Fe/Fe_3O_4 bimagnetic nanoparticles (MNPs); (2) the MNPs accumulate with time as aggregates in the cytosol; (3) the MNPs cause minimal toxicity in those cells; (4) NPCs loaded with MNPs travel to subcutaneous melanomas; (5) after A/C magnetic field exposure, the targeted delivery of MNPs by the cells results in a significant regression of the tumors; and (6) this treatment results in apoptosis of cancer cells and alters the tumor proteome. The tumor attenuation was significant ($p < 0.05$) 96 h after the last of three AMF exposures.

The goal of many current therapeutic strategies is to avoid the deleterious and sometimes catastrophic side effects associated with chemotherapeutic intervention. The stealth delivery system described above for targeted hyperthermia of tumors offers the prospect for more specific tumor ablation. Although the melanoma model used here was a subcutaneous one, deep metastatic lesions could potentially be targeted in a similar manner using a lower frequency A/C magnetic field. Adjunct targeted chemotherapy using therapeutic agents coupled to the MNPs or encased within liposomes such as those reported by Ikehara *et al.*[46] may further enhance this platform for future use in targeted application to human cancer therapy.

MATERIALS AND METHODS

Synthesis of Fe/Fe_3O_4 Nanoparticles. The synthesis of Fe/Fe_3O_4 NPs is proprietary information of NanoScale Corporation, Manhattan, KS.

Porphyrin-Tethered Stealth-Coated (Bi) Magnetic Fe/Fe_3O_4 Nanoparticles. Aminosiloxane-coated Fe/Fe_3O_4 core/shell nanoparticles were synthesized by NanoScale Corporation (Manhattan, KS); the synthesis is represented in Scheme 1.

Synthesis of Fe/Fe_3O_4/ASOX. The synthesis of ASOX-covered Fe/Fe_3O_4 NPs was performed by adapting a procedure from the literature.[63] Twenty milligrams of Fe/Fe_3O_4 nanoparticles were suspended in 10 mL of anhydrous tetrahydrofuran (THF). After sonicating, the undissolved solid (<1 mg) was separated by precipitation through low-speed centrifugation (1500 rpm, 5 min). The clear solution was transferred to another test tube and 3-aminopropyltriethoxylsilane (see Scheme 1) was added to the solution. After sonicating, the nanoparticles were collected by high speed centrifugation (15 000 rpm for 15 min). After redispersion and subsequent collection in THF, the Fe/Fe_3O_4/ASOX-NPs (7.5 mg) were collected, dried in high vacuum, and stored under argon.

Synthesis of Stealth-Coated Fe/Fe_3O_4/ASOX Nanoparticles. Forty milligrams of dopamine-based ligand (see Scheme 1) was dissolved in 5.0 mL of THF, and 20 mg of Fe/Fe_3O_4/ASOX nanoparticles, and 1.0 g of CDI (carbonyl diimidazole) were added as solids. After sonicating, the nanoparticles were collected by high speed centrifugation (15 000 rpm for 15 min). After redispersion and subsequent collection in THF, the Fe/Fe_3O_4/stealth NPs (15 mg) were collected, dried in high vacuum, and stored under argon.

Synthesis of TCPP-Linked Stealth-Coated Fe/Fe_3O_4/ASOX Nanoparticles. TCPP (tetrakis(4-carboxyphenyl)porphyrin) (2.5 mg) was dissolved in 5.0 mL of THF; 20 mg of Fe/Fe_3O_4/ASOX/stealth nanoparticles and 1.0/0.05 g of EDC/HOBT (1-ethyl-3-(3-dimethylaminopropyl)carbodiimide/1-hydroxybenzotriazole) were added as solids.[64] After sonicating, the nanoparticles were collected by high speed centrifugation (15 000 rpm for 15 min). After redispersion and subsequent collection in THF, the TCPP-labeled Fe/Fe_3O_4/ASOX/stealth NPs (13.5 mg) were collected, dried in high vacuum, and stored under argon. We have determined by using UV/vis spectroscopy (λ_{abs}(TCPP) = 416 nm, = 365 000 M^{-1} cm^{-1}) that 5 ± 0.5 TCPP units are bound to one stealth-coated Fe/Fe_3O_4/ASOX nanoparticle, on average.

As already stated, HRTEM performed at the University of Kansas Microscopy and Analytical Imaging Laboratories has revealed that the nanoparticles are composed of nanorods (5−10 nm in length, 1−4 nm in diameter). These nanorods form clusters of 16.0 ± 1.5 nm in diameter. The thickness of the aminosiloxane shell that is surrounding the whole Fe/Fe_3O_4 clusters is 2.0 ± 0.4 nm. This is consistent with an average diameter of the Fe/Fe_3O_4/ASOX nanoparticles of 20 ± 2.3 nm. Using the program IMAGE (NIH), we have determined the polydispersity index of the Fe/Fe_3O_4/ASOX nanoparticles to be 1.15. Note that the stealth ligand has a length of 2.5 nm (AM1, Chemdraw Ultra 3D package, Cambridge Soft Corporation, Cambridge, MA), so that the resulting Fe/Fe_3O_4/ASOX stealth nanoparticles are 25 ± 2.3 nm in size. The space demand for the dopamine anchor is 1.094 nm^2 (AM1). One Fe/Fe_3O_4/ASOX nanoparticle of 20 nm in diameter can bind 1150 organic ligands. The porphyrin labels have a diameter of 1.95 nm (AM1). The binding of the ligands to the terminal amino groups of the aminosiloxane layer was achieved in THF under argon in the presence of CDI as coupling reagent; the molar ratio of ligands L1/L1-TCPP was 1000/3.5. We assume a statistical distribution of the ligands at the surface. Assuming a Poisson distribution,[65] 99.33% of the Fe/Fe_3O_4/ASOX/stealth NPs at

the chosen ratio (5 TCPP units per nanoparticle) feature at least one chemically linked TCPP unit. The solubility of the organically coated Fe/Fe_3O_4 NPs was determined to be 2.25 mg mL^{-1} and the specific adsorption rate (SAR) at the field conditions described here was 620 ± 30 Wg^{-1} (Fe). We have determined the zeta-potential of the Fe/Fe_3O_4/ASOX/stealth TCPP nanoparticles by using Zeta Plus (Brookhaven Instruments, Holtsville, NY) to be 34 mV in 0.1 M PBS buffer at 298 K; their BET surface was determined in NanoScale Corporation's analytical laboratory to be 72 ± 2 $m^2 g^{-1}$.

Tissue Culture of C17.2 Neural Progenitor Cells and B16-F10 Melanoma Cells. B16-F10 melanoma cells were purchased from ATCC (Manassas, VA) and maintained in Dulbecco's modified Eagle medium (DMEM; Invitrogen, Carlsbad, CA) supplemented with 10% fetal bovine serum (FBS; Sigma-Aldrich, St. Louis, MO) and 1% penicillin/streptomycin (Invitrogen) at 37 °C in a humidified atmosphere containing 5% carbon dioxide.

C17.2 neural progenitor cells (NPCs) were a gift from V Ourednik (Iowa State University). Originally developed in Evan Snyder's lab,[66] these cells were maintained in DMEM supplemented with 10% FBS (Sigma-Aldrich), 5% horse serum (Invitrogen), 1% glutamine (Invitrogen), and 1% penicillin/streptomycin (Invitrogen).

Cytotoxicity of MNPs on Neural Progenitor Cells and B16-F10 Cells. Potential cytotoxic effects of MNPs (NanoScale Corporation, Manhattan, KS) were studied by incubating C17.2 NPCs and B16-F10 melanoma cells in different concentrations of MNPs (as determined by iron content). NPCs and B16-F10 cells were plated at 50 000 cells/cm^2 and incubated overnight with their respective media containing MNPs at concentrations of 5, 10, 15, 20, or 25 μg/mL iron. After incubation, medium was removed and cells were washed twice with DMEM. Cells were lifted *via* trypsinization, and live and dead cell numbers were counted *via* hemocytometer with Trypan blue staining. This method allows counting of viable (colorless) and nonviable (blue stained) cells since only the dead cells allow the blue stain into the cell. A photograph of Trypan blue stained cells showing the blue coloration of dead cells in the hemocytometer grid is shown in Figure S2 (Supporting Information). NPCs and B16-F10 cells were used in three separate trials, and each experiment was done in triplicate.

Prussian Blue Staining on NPCs. The loading efficiency of MNPs into NPCs was assessed using Perl's Prussian blue stain kit (Polysciences, Inc., Warrington, PA). After overnight incubation in NPC medium containing 25 μg/mL iron in MNPs, NPCs were washed twice with DMEM and PBS and fixed with 4% glutaraldehyde for 10 min. Fixed NPCs were incubated in a solution containing equal amounts of 4% potassium ferrocyanide and 4% HCl for 20 min. After 20 min incubation, NPCs were washed twice with 1× PBS and counterstained with nuclear fast red solution for 30 min. Images were captured using a Zeiss Axiovert 40 CFL microscope (New York) and a Jenoptik ProgRes C3 camera (Jena, Germany).

Loading Strategy of MNPs and Determination of Iron Amounts. The loading efficiency of NPCs with various iron concentrations of MNPs was determined spectrophotometrically using a Ferrozine iron estimation method.[67] For this method, cells were incubated overnight with NPC medium containing different concentrations of MNPs and then washed twice with DMEM and 1× PBS. Cells in medium without MNPs were used as controls. All NPCs (control cells and cells loaded with various iron concentration of MNPs) were trypsinized, counted, and centrifuged, and total cells were resuspended in 2 mL of distilled water. Cells were then lysed by adding 0.5 mL of 1.2 M HCl and 0.2 mL of 2 M ascorbic acid and incubating at 65−70 °C for 2 h. After 2 h, 0.2 mL of reagent containing 6.5 mM Ferrozine (HACH, Loveland, CO), 13.1 mM neocuproine (Sigma-Aldrich, St. Louis, MO), 2 M ascorbic acid (Alfa Aesar, Ward Hill, MA), and 5 M ammonium acetate (Sigma-Aldrich, St. Louis, MO) was added and incubated for 30 min at room temperature. After 30 min, samples were centrifuged at 1000 rpm for 5 min, and supernatant optical density was measured by a UV−vis spectrophotometer (Shimadzu, Columbia, MD) at 562 nm. A standard curve was prepared using 0, 0.1, 0.2, 0.5, 1, 2, and 5 μg/mL ferrous ammonium sulfate samples. Water with all other reagents was used as a blank. From the standard curve, iron concentration in cell samples was determined. Iron concentration per single cell was estimated by dividing the iron amount in each cell sample by the total number of cells in that sample.

AMF-Induced Temperature Changes *In Vitro*. To verify the temperature increase by NPCs loaded with MNPs in a simulated tumor environment, NPCs were loaded overnight with MNPs equivalent to 15 μg/mL Fe. After incubation, cells were washed twice with DMEM and twice with 1× PBS to remove free MNPs. Cells were lifted with 0.1% trypsin-EDTA, and 1 × 10^6 cells were pelleted by centrifugation in 2 mL centrifuge tubes; 1.5 mL of 4% agarose solution was added on top of the cell pellet to mimic the extracellular matrix in tumor tissues. Agarose centrifuge tubes containing pelleted NPCs without MNPs were used as negative controls and were made as described above. The experiment was conducted in triplicate. Before each tube was exposed to AMF, two optical probes (Neoptix, Quebec, Canada) were inserted into the tube: one at the pellet, and the second one at the middle of the agarose. Tubes were exposed to AMF for 10 min, and the temperature difference over time was measured by the probes.

Evaluation of Selective Engraftment of NPCs and Magnetic Hyperthermia. Female, 6−8 week old, C57BL/6 mice were purchased from Charles River Laboratories (Wilmington, MA). Mice were held for 1 week after arrival to allow them to acclimate. Mice were maintained according to approved IACUC guidelines in the Comparative Medicine Group facility of Kansas State University. All animal experiments were conducted according to these IACUC guidelines. On day 0, 3.5 × 10^5 B16-F10 melanoma cells were injected subcutaneously into 21 C57BL/6 mice, and the mice were randomly divided into three groups. On day 5, 1 × 10^6 NPCs loaded with MNPs at 20 μg/mL iron concentration were injected intravenously to two groups (NPC-MNP, group I; and NPC-MNP+AMF, group II); simultaneously, saline was injected into group III. On the ninth, 10th, and 11th days after tumor inoculation, group II mice with NPC-loaded MNPs were exposed to AMF for 10 min daily using an alternating magnetic field apparatus (Superior Induction Company, Pasadena, CA). The frequency is fixed (366 kHz, sine wave pattern); field amplitude is 5 kA/m. Tumor volumes were measured using a caliper on days 8, 10, and 12; they were calculated using the formula $0.5a \times b^2$, where a is the larger diameter and b the smaller diameter of the tumor. All of the mice were then euthanized on day 15, and the tissues were collected. The experiment was repeated once with similar results.

Histological Analysis. All mice were sacrificed 15 days after tumor inoculation by CO_2 inhalation and cervical dislocation. Tumor, lung, liver, and spleen were snap-frozen in liquid nitrogen for histological analysis. Tissues were sectioned on a cryostat (Leitz Kryostat 1720, Germany) at 8−10 μm and used for histological studies. Prussian blue staining was performed on these sections using Perl's Prussian blue stain kit to identify NPCs loaded with MNPs. Apoptotic cell detection in the tissue sections was determined using the DeadEnd fluorometric terminal deoxynucleotidyl transferase dUTP nick end labeling (TUNEL) system (Promega Corporation, Madison, WI), as per the manufacturer's protocol.

Protein Preparation for Two-Dimensional Electrophoresis (2-DE). To identify protein expression differences between tumors from mice receiving AMF after IV saline injection or after IV NPC-MNP injection, 3.5 × 10^5 B16-F10 melanoma cells were injected subcutaneously into two mice. On day 5, 1 × 10^6 NPCs loaded with MNPs at 20 μg/mL iron concentration were injected intravenously into one mouse; simultaneously, saline was injected into the other mouse. On days 9, 10, and 11, tumors were exposed to AMF. On day 11, mice were euthanized and tumors were collected immediately after AMF exposure.

Total protein was prepared from the tumors for use in two-dimensional gel electrophoresis (2-DE) analysis. The following protein isolation protocol was used.[68] Briefly, melanoma tissues were homogenized using a Pellet Pestle Mortar (KONTES, Vineland, NJ) in the presence of 0.5 mL of lysis buffer (8 M urea, 2 M thiourea, 4% 3-cholamidopropyldimethylammonio-1-propanesulfonate (CHAPS), 100 mM dithiothreitol (DTT), 25 mM Tris-Cl, and 0.2% ampholyte (pH 3−10) (Amersham Pharmacia Biotech, Piscataway, NJ). The supernatant was collected and then

precipitated using 2 volumes of ice-cold acetone. The final protein pellet was dissolved in 100 μL of the sample buffer (8 M urea, 2 M thiourea, 4% CHAPS, 100 mM DTT, 25 mM Tris-Cl, and 0.2% ampholyte (pH 3−10)). Protein concentrations were determined using a reducing agent-compatible and detergent-compatible protein assay kit (Bio-Rad, Hercules, CA).

2-DE Analysis. Fifty micrograms of total protein was resolved at 20 °C in the first dimension by isoelectric focusing (IEF) in an IEF cell system (Bio-Rad, Hercules, CA) using 7 cm long, pH 3−10, precast immobilized pH gradient strips (Bio-Rad). The IEF parameters were 250 V for 15 min, followed by 4000 V for 5 h. At the end of the IEF, the strips were equilibrated sequentially for 10 min each in 1 mL of equilibration buffer I (375 mM Tris-HCl [pH 8.8], 6 M urea, 2% sodium dodecyl sulfate (SDS), 2% DTT) and buffer II (375 mM Tris-HCl [pH 8.8], 6 M urea, 2% SDS, 2.72 mg of iodoacetamide/mL, 0.001% bromophenol blue). Subsequently, second-dimension SDS-polyacrylamide gel electrophoresis analysis was performed on the strips in a Mini-PROTEAN Tetra system by using 12% polyacrylamide gels (Bio-Rad) for 40 min at 200 V at room temperature in a 50 mM Tris-glycine buffer. The 2-DE resolved gels were stained by using a Biosafe Coomassie G-250 kit (Bio-Rad). Coomassie stained gels were digitalized by using an HP Scanjet 7400c scanner (Hewlett-Packard, Houston, TX).

Matrix-Assisted Laser Desorption Ionization (MALDI)-TOF MS Analysis of Melanoma Tissues Treated with AMF and AMF with NSC-MNP Proteins. After resolution by 2-DE, proteins from melanomas from mice treated with AMF and MNP-NPC+AMF were picked individually from Coomassie blue stained gels using PROTEINEER spII with sp-Control 3.0 software (Bruker Daltonics, Bremen, Germany) according to the manufacturer's protocol. Coomassie blue stained proteins were digested as described by Shevchenko *et al.*[68] An aliquot of in-gel-digested solution was mixed with an equal volume of a saturated solution of 1 μL of 2,5-dihydroxybenzoic acid (DHB) in 50% aqueous acetonitrile, and 1 μL of mixture was spotted onto a target plate. Protein analysis was performed with a Bruker UltraFlex II MALDI-TOF using MTP AnchorChip with 384 matrix spots. MALDI-TOF spectra were externally calibrated using a combination of nine standard peptides: bradykinin 1-7 (757.39 Da), angiotensin II (1046.54 Da), angiotensin I (1296.68 Da), neurotensin (1672.91 Da), renin substrate (1758.93 Da), ACTH clip 1-17 (2093.08 Da), ACTH clip 18-39 (2465.19 Da), ACTH clip 1-24 (2932.58 Da), and ACTH clip 7-38 (3657.92 Da), spotted onto positions adjacent to the samples. Protein identification was carried out by automatic comparison of experimentally generated monoisotopic values of peptides using MASCOT with a tolerance of 0.5−0.3 Da and 0−1 missed cleavage, and oxidation of methionine was allowed.

Statistical Analysis. Statistical analyses were performed using WinSTAT (A-Prompt Corporation, Lehigh Valley, PA). The means of the experimental groups were evaluated to confirm that they met the normality assumption. To evaluate the significance of overall differences in tumor volumes between all *in vivo* groups, statistical analysis was performed by analysis of variance (ANOVA). A p value less than 0.1 was considered as significant. Following significant ANOVA, *post hoc* analysis using least significance difference (LSD) was used for multiple comparisons. Significance for *post hoc* testing was set at $p < 0.05$. All of the tumor volume data are represented as mean ± standard error (SE) on graphs.

Acknowledgment. This work was supported by NIH 1R21CA135599, NSF IIP 0930673, HHSN261200800059C from the Small Business Innovation Research Development Center (SBIR) of the National Cancer Institute, the Terry C. Johnson Center for Basic Cancer Research at Kansas State University, Kansas State University Targeted Excellence, Kansas State Legislative Appropriation, and Kansas Agricultural Experiment Station. We would also like to thank Dr. J. Tomich (Biotechnology/Proteomics Core lab) from Kansas State University for the use of his core facility, and Dr. D. Moore of the University of Kansas Microscopy and Analytical Imaging Laboratory for his assistance with HRTEM.

Supporting Information Available: Supplemental Figures S1 and S2 show a TEM image of MNPs and a photo of a hemacytometer grid with trypan blue stained, MNP-loaded NPCs, respectively. This material is available free of charge *via* the Internet at http://pubs.acs.org.

REFERENCES AND NOTES

1. Giammarioli, A. M.; Maselli, A.; Casagrande, A.; Gambardella, L.; Gallina, A.; Spada, M.; Giovannetti, A.; Proietti, E.; Malorni, W.; Pierdominici, M. Pyrimethamine Induces Apoptosis of Melanoma Cells *via* a Caspase and Cathepsin Double-Edged Mechanism. *Cancer Res.* **2008**, *68*, 5291–300.
2. Liu, Y.; Zhang, W.; Niu, T.; Cheung, L. H.; Munshi, A.; Meyn, R. E., Jr.; Rosenblum, M. G. Targeted Apoptosis Activation with GrB/ScFvMEL Modulates Melanoma Growth, Metastatic Spread, Chemosensitivity, and Radiosensitivity. *Neoplasia* **2006**, *8*, 125–135.
3. Sato, M.; Yamashita, T.; Ohkura, M.; Osai, Y.; Sato, A.; Takada, T.; Matsusaka, H.; Ono, I.; Tamura, Y.; Sato, N.; *et al.* *N*-Propionyl-Cysteaminylphenol-Magnetite Conjugate (NPrCAP/M) Is a Nanoparticle for the Targeted Growth Suppression of Melanoma Cells. *J. Invest. Dermatol.* **2009**, *129*, 2233–2241.
4. Gordon, R. T.; Hines, J. R.; Gordon, D. Intracellular Hyperthermia. A Biophysical Approach to Cancer Treatment *via* Intracellular Temperature and Biophysical Alterations. *Med. Hypotheses* **1979**, *5*, 83–102.
5. Shellman, Y. G.; Howe, W. R.; Miller, L. A.; Goldstein, N. B.; Pacheco, T. R.; Mahajan, R. L.; LaRue, S. M.; Norris, D. A. Hyperthermia Induces Endoplasmic Reticulum-Mediated Apoptosis in Melanoma and Non-melanoma Skin Cancer Cells. *J. Invest. Dermatol.* **2008**, *128*, 949–956.
6. Coffey, D. S.; Getzenberg, R. H.; DeWeese, T. L. Hyperthermic Biology and Cancer Therapies: A Hypothesis for the "Lance Armstrong Effect". *JAMA* **2006**, *296*, 445–448.
7. Jones, E. L.; Oleson, J. R.; Prosnitz, L. R.; Samulski, T. V.; Vujaskovic, Z.; Yu, D.; Sanders, L. L.; Dewhirst, M. W. Randomized Trial of Hyperthermia and Radiation for Superficial Tumors. *J. Clin. Oncol.* **2005**, *23*, 3079–3085.
8. Wust, P.; Gneveckow, U.; Johannsen, M.; Bohmer, D.; Henkel, T.; Kahmann, F.; Sehouli, J.; Felix, R.; Ricke, J.; Jordan, A. Magnetic Nanoparticles for Interstitial Thermotherapy—Feasibility, Tolerance and Achieved Temperatures. *Int. J. Hyperthermia* **2006**, *22*, 673–685.
9. Cavaliere, R.; Ciocatto, E. C.; Giovanella, B. C.; Heidelberger, C.; Johnson, R. O.; Margottini, M.; Mondovi, B.; Moricca, G.; Rossi-Fanelli, A. Selective Heat Sensitivity of Cancer Cells. Biochemical and Clinical Studies. *Cancer* **1967**, *20*, 1351–1381.
10. Gao, J.; Gu, H.; Xu, B. Multifunctional Magnetic Nanoparticles: Design, Synthesis, and Biomedical Applications. *Acc. Chem. Res.* **2009**, *42*, 1097–1107.
11. Salloum, M.; Ma, R.; Zhu, L. An *In Vivo* Experimental Study of Temperature Elevations in Animal Tissue During Magnetic Manoparticle Hyperthermia. *Int. J. Hyperthermia* **2008**, *24*, 589–601.
12. Salloum, M.; Ma, R. H.; Weeks, D.; Zhu, L. Controlling Nanoparticle Delivery in Magnetic Nanoparticle Hyperthermia for Cancer Treatment: Experimental Study in Agarose Gel. *Int. J. Hyperthermia* **2008**, *24*, 337–345.
13. Jordan, A.; Wust, P.; Fahling, H.; John, W.; Hinz, A.; Felix, R. Inductive Heating of Ferrimagnetic Particles and Magnetic Fluids: Physical Evaluation of Their Potential for Hyperthermia. *Int. J. Hyperthermia* **1993**, *9*, 51–68.
14. Kalambur, V. S.; Longmire, E. K.; Bischof, J. C. Cellular Level Loading and Heating of Superparamagnetic Iron Oxide Nanoparticles. *Langmuir* **2007**, *23*, 12329–12336.
15. Shinkai, M. Functional Magnetic Particles for Medical Application. *J. Biosci. Bioeng.* **2002**, *94*, 606–613.
16. Balivada, S.; Rachakatla, R. S.; Wang, H.; Samarakoon, T. N.; Dani, R. K.; Pyle, M.; Kroh, F. O.; Walker, B.; Leaym, X.; Koper, O. B.; *et al.* A/C Magnetic Hyperthermia of Melanoma Mediated by Iron(0)/Iron Oxide Core/Shell Magnetic Nanoparticles: A Mouse Study. *BMC Cancer* **2010**, *10*, 119.

17. Bagheri, S.; Nosrati, M.; Li, S.; Fong, S.; Torabian, S.; Rangel, J.; Moore, D. H.; Federman, S.; Laposa, R. R.; Baehner, F. L.; *et al.* Genes and Pathways Downstream of Telomerase in Melanoma Metastasis. *Proc. Natl. Acad. Sci. U.S.A.* **2006**, *103*, 11306–11311.
18. Haqq, C.; Nosrati, M.; Sudilovsky, D.; Crothers, J.; Khodabakhsh, D.; Pulliam, B. L.; Federman, S.; Miller, J. R., III; Allen, R. E.; Singer, M. I.; *et al.* The Gene Expression Signatures of Melanoma Progression. *Proc. Natl. Acad. Sci. U.S.A.* **2005**, *102*, 6092–6097.
19. Kashani-Sabet, M.; Rangel, J.; Torabian, S.; Nosrati, M.; Simko, J.; Jablons, D. M.; Moore, D. H.; Haqq, C.; Miller, J. R., III; Sagebiel, R. W. A Multi-marker Assay To Distinguish Malignant Melanomas from Benign Nevi. *Proc. Natl. Acad. Sci. U.S.A.* **2009**, *106*, 6268–6272.
20. Chen, J. H.; Ni, R. Z.; Xiao, M. B.; Guo, J. G.; Zhou, J. W. Comparative Proteomic Analysis of Differentially Expressed Proteins in Human Pancreatic Cancer Tissue. *Hepatobiliary Pancreatic Dis. Int.* **2009**, *8*, 193–200.
21. Chen, R.; Pan, S.; Aebersold, R.; Brentnall, T. A. Proteomics Studies of Pancreatic Cancer. *Proteomics: Clin. Appl.* **2007**, *1*, 1582–1591.
22. Chen, Y.; Ouyang, G. L.; Yi, H.; Li, M. Y.; Zhang, P. F.; Li, C.; Li, J. L.; Liu, Y. F.; Chen, Z. C.; Xiao, Z. Q. Identification of RKIP as an Invasion Suppressor Protein in Nasopharyngeal Carcinoma by Proteomic Analysis. *J. Proteome Res.* **2008**, *7*, 5254–5262.
23. Dilnawaz, F.; Singh, A.; Mohanty, C.; Sahoo, S. K. Dual Drug Loaded Superparamagnetic Iron Oxide Nanoparticles for Targeted Cancer Therapy. *Biomaterials* **2010**, *31*, 3694–3706.
24. Chen, Y.; Zhu, X.; Zhang, X.; Liu, B.; Huang, L. Nanoparticles Modified with Tumor-Targeting ScFv Deliver SiRNA and MiRNA for Cancer Therapy. *Mol. Ther.* **2010**, *18*, 1650–1656.
25. Agemy, L.; Sugahara, K. N.; Kotamraju, V. R.; Gujraty, K.; Girard, O. M.; Kono, Y.; Mattrey, R. F.; Park, J. H.; Sailor, M. J.; Jimenez, A. I.; *et al.* Nanoparticle-Induced Vascular Blockade in Human Prostate Cancer. *Blood* **2010**, *116*, 2847–2856.
26. Sugahara, K. N.; Teesalu, T.; Karmali, P. P.; Kotamraju, V. R.; Agemy, L.; Girard, O. M.; Hanahan, D.; Mattrey, R. F.; Ruoshlati, E. Tissue-Penetrating Delivery of Compounds and Nanoparticles into Tumors. *Cancer Cell* **2009**, *16*, 510–520.
27. Sugahara, K. N.; Teesalu, T.; Karmali, P. P.; Kotamraju, V. R.; Agemy, L.; Greenwald, D. R.; Ruoshlati, E. Coadministration of a Tumor-Penetrating Peptide Enhances the Efficacy of Cancer Drugs. *Science* **2010**, *328*, 1031–1035.
28. Aboody, K. S.; Brown, A.; Rainov, N. G.; Bower, K. A.; Liu, S.; Yang, W.; Small, J. E.; Herrlinger, U.; Ourednik, V.; Black, P. M.; *et al.* Neural Stem Cells Display Extensive Tropism for Pathology in Adult Brain: Evidence from Intracranial Gliomas. *Proc. Natl. Acad. Sci. U.S.A.* **2000**, *97*, 12846–12851.
29. Aboody, K. S.; Bush, R. A.; Garcia, E.; Metz, M. Z.; Najbauer, J.; Justus, K. A.; Phelps, D. A.; Remack, J. S.; Yoon, K. J.; Gillespie, S.; *et al.* Development of a Tumor-Selective Approach To Treat Metastatic Cancer. *PLoS One* **2006**, *1*, e23.
30. Aboody, K. S.; Najbauer, J.; Schmidt, N. O.; Yang, W.; Wu, J. K.; Zhuge, Y.; Przylecki, W.; Carroll, R.; Black, P. M.; Perides, G. Targeting of Melanoma Brain Metastases Using Engineered Neural Stem/Progenitor Cells. *Neuro. Oncol.* **2006**, *8*, 119–126.
31. Rachakatla, R. S.; Marini, F.; Weiss, M. L.; Tamura, M.; Troyer, D. Development of Human Umbilical Cord Matrix Stem Cell-Based Gene Therapy for Experimental Lung Tumors. *Cancer Gene Ther.* **2007**, *14*, 828–835.
32. Rachakatla, R. S.; Pyle, M. M.; Ayuzawa, R.; Edwards, S. M.; Marini, F. C.; Weiss, M. L.; Tamura, M.; Troyer, D. Combination Treatment of Human Umbilical Cord Matrix Stem Cell-Based Interferon-β Gene Therapy and 5-Fluorouracil Significantly Reduces Growth of Metastatic Human Breast Cancer in SCID Mouse Lungs. *Cancer Invest.* **2008**, *26*, 662–670.
33. Loebinger, M. R.; Kyrtatos, P. G.; Turmaine, M.; Price, A. N.; Pankhurst, Q.; Lythgoe, M. F.; Janes, S. M. Magnetic Resonance Imaging of Mesenchymal Stem Cells Homing to Pulmonary Metastases Using Biocompatible Magnetic Nanoparticles. *Cancer Res.* **2009**, *69*, 8862–8867.
34. Gillies, R. J.; Martinez-Zaguilan, R.; Martinez, G. M.; Serrano, R.; Perona, R. Tumorigenic 3T3 Cells Maintain an Alkaline Intracellular pH Under Physiological Conditions. *Proc. Natl. Acad. Sci. U.S.A.* **1990**, *87*, 7414–7418.
35. Ehtesham, M.; Kabos, P.; Kabosova, A.; Neuman, T.; Black, K. L.; Yu, J. S. The Use of Interleukin 12-Secreting Neural Stem Cells for the Treatment of Intracranial Glioma. *Cancer Res.* **2002**, *62*, 5657–5663.
36. Lazarini, F.; Tham, T. N.; Casanova, P.; Arenzana-Seisdedos, F.; Dubois-Dalcq, M. Role of the α-Chemokine Stromal Cell-Derived Factor (SDF-1) in the Developing and Mature Central Nervous System. *Glia* **2003**, *42*, 139–148.
37. Wu, X.; Hu, J.; Zhou, L.; Mao, Y.; Yang, B.; Gao, L.; Xie, R.; Xu, F.; Zhang, D.; Liu, J.; Zhu, J. *In Vivo* Tracking of Superparamagnetic Iron Oxide Nanoparticle-Labeled Mesenchymal Stem Cell Tropism to Malignant Gliomas Using Magnetic Resonance Imaging. Laboratory Investigation. *J. Neurosurg.* **2008**, *108*, 320–329.
38. Muehlberg, F. L.; Song, Y. H.; Krohn, A.; Pinilla, S. P.; Droll, L. H.; Leng, X.; Seidensticker, M.; Ricke, J.; Altman, A. M.; Devarajan, E.; *et al.* Tissue-Resident Stem Cells Promote Breast Cancer Growth and Metastasis. *Carcinogenesis* **2009**, *30*, 589–597.
39. Studeny, M.; Marini, F. C.; Champlin, R. E.; Zompetta, C.; Fidler, I. J.; Andreeff, M. Bone Marrow-Derived Mesenchymal Stem Cells as Vehicles for Interferon-β Delivery into Tumors. *Cancer Res.* **2002**, *62*, 3603–3608.
40. Kucerova, L.; Altanerova, V.; Matuskova, M.; Tyciakova, S.; Altaner, C. Adipose Tissue-Derived Human Mesenchymal Stem Cells Mediated Prodrug Cancer Gene Therapy. *Cancer Res.* **2007**, *67*, 6304–6313.
41. Rachakatla, R. S.; Marini, F.; Weiss, M. L.; Tamura, M.; Troyer, D. Development of Human Umbilical Cord Matrix Stem Cell-Based Gene Therapy for Experimental Lung Tumors. *Cancer Gene Ther.* **2007**, *14*, 828–835.
42. Rachakatla, R. S.; Pyle, M. M.; Ayuzawa, R.; Edwards, S. M.; Marini, F. C.; Weiss, M. L.; Tamura, M.; Troyer, D. Combination Treatment of Human Umbilical Cord Matrix Stem Cell-Based Interferon-β Gene Therapy and 5-Fluorouracil Significantly Reduces Growth of Metastatic Human Breast Cancer in SCID Mouse Lungs. *Cancer Invest.* **2008**, *26*, 662–670.
43. Rachakatla, R. S.; Troyer, D. Wharton's Jelly Stromal Cells as Potential Delivery Vehicles for Cancer Therapeutics. *Future Oncol.* **2009**, *5*, 1237–1244.
44. Winterbourn, C. C. Toxicity of Iron and Hydrogen Peroxide: the Fenton Reaction. *Toxicol. Lett.* **1995**, *82*−*83*, 969–974.
45. Kroh, F. O. In Small Business Innovation Research Development Center (SBIR) of the National Cancer Institute: HHSN261200800059C.
46. Ikehara, Y.; Niwa, T.; Biao, L.; Ikehara, S. K.; Ohashi, N.; Kobayashi, T.; Shimizu, Y.; Kojima, N.; Nakanishi, H. A Carbohydrate Recognition-Based Drug Delivery and Controlled Release System Using Intraperitoneal Macrophages as a Cellular Vehicle. *Cancer Res.* **2006**, *66*, 8740–8748.
47. Huber, D. L. Synthesis, Properties, and Applications of Iron Nanoparticles. *Small* **2005**, *1*, 482–501.
48. Jain, T.; Morales, M. M.; Sakoo, S. K.; Leslie-Pelecky, D. L.; Labhasetwar, V. Iron Oxide Nanoparticles for Sustained Delivery of Anticancer Agents. *Mol. Pharm.* **2005**, *2*, 194–205.
49. Bossmann, S. H. Nanoparticles for Hyperthermia Treatment of Cancer. *Fabrication and Bio-Application of Functionalized Nanomaterials*; Research Signpost/Transworld Research Network; Trivandrum, Kerala, India, 2009; pp 171−206.
50. Cho, J. A.; Park, H.; Kim, H. K.; Lim, E. H.; Seo, S. W.; Choi,

J. S.; Lee, K. W. Hyperthermia-Treated Mesenchymal Stem Cells Exert Antitumor Effects on Human Carcinoma Cell Line. *Cancer* **2009**, *115*, 311–323.
51. Park, H.; Cho, J. A.; Kim, S. K.; Kim, J. H.; Lee, S. H. Hyperthermia on Mesenchymal Stem Cells (MSCs) Can Sensitize Tumor Cells To Undergo Cell Death. *Int. J. Hyperthermia* **2008**, *24*, 638–648.
52. Multhoff, G. Activation of Natural Killer Cells by Heat Shock Protein 70. *Int. J. Hyperthermia* **2002**, *18*, 576–585.
53. Fierro, M. T.; Liao, X. S.; Lusso, P.; Bonferroni, M.; Matera, L.; Cesano, A.; Lista, P.; Arione, R.; Forni, G.; Foa, R. *In Vitro* and *In Vivo* Susceptibility of Human Leukemic Cells to Lymphokine Activated Killer Activity. *Leukemia* **1988**, *2*, 50–54.
54. Kubes, J.; Svoboda, J.; Rosina, J.; Starec, M.; Fiserova, A. Immunological Response in the Mouse Melanoma Model after Local Hyperthermia. *Physiol. Res.* **2008**, *57*, 459–465.
55. Tang, S. J.; Ho, M. Y.; Cho, H. C.; Lin, Y. C.; Sun, G. H.; Chi, K. H.; Wang, Y. S.; Jhou, R. S.; Yang, W.; Sun, K. H. Phosphoglycerate Kinase 1-Overexpressing Lung Cancer Cells Reduce Cyclooxygenase 2 Expression and Promote Anti-Tumor Immunity *In Vivo*. *Int. J. Cancer* **2008**, *123*, 2840–2848.
56. Wang, J.; Ying, G.; Jung, Y.; Lu, J.; Zhu, J.; Pienta, K. J.; Taichman, R. S. Characterization of Phosphoglycerate Kinase-1 Expression of Stromal Cells Derived from Tumor Microenvironment in Prostate Cancer Progression. *Cancer Res.* , *70*, 471–480.
57. Nakano, H.; Oshima, H.; Chung, W.; Williams-Abbott, L.; Ware, C. F.; Yagita, H.; Okumura, K. TRAF5, an Activator of NF-κB and Putative Signal Transducer for the Lymphotoxin-β Receptor. *J. Biol. Chem.* **1996**, *271*, 14661–14664.
58. Gibbs, P. E.; Maines, M. D. Biliverdin Inhibits Activation of NF-κB: Reversal of Inhibition by Human Biliverdin Reductase. *Int. J. Cancer* **2007**, *121*, 2567–2574.
59. Wu, K.; Bonavida, B. The Activated NF-κB-Snail-RKIP Circuitry in Cancer Regulates Both the Metastatic Cascade and Resistance to Apoptosis by Cytotoxic Drugs. *Crit. Rev. Immunol.* **2009**, *29*, 241–254.
60. Melle, C.; Ernst, G.; Scheibner, O.; Kaufmann, R.; Schimmel, B.; Bleul, A.; Settmacher, U.; Hommann, M.; Claussen, U.; von Eggeling, F. Identification of Specific Protein Markers in Microdissected Hepatocellular Carcinoma. *J. Proteome Res.* **2007**, *6*, 306–315.
61. Selga, E.; Noe, V.; Ciudad, C. J. Transcriptional Regulation of Aldo-Keto Reductase 1C1 in HT29 Human Colon Cancer Cells Resistant to Methotrexate: Role in the Cell Cycle and Apoptosis. *Biochem. Pharmacol.* **2008**, *75*, 414–426.
62. Maines, M. D.; Mayer, R. D.; Erturk, E.; Huang, T. J.; Disantagnese, A. The Oxidoreductase, Biliverdin Reductase, Is Induced in Human Renal Carcinoma—pH and Cofactor-Specific Increase in Activity. *J. Urol.* **1999**, *162*, 1467–1472.
63. Li, Y. S.; Church, J. S.; Woodhead, A. L.; Moussa, F. Preparation and Characterization of Silica Coated Iron Oxide Magnetic Nano-Particles. *Spectrochim. Acta A* , *76*, 484–489.
64. Clarke, S. E.; Wamser, C. C.; Bell, H. E. Aqueous Complexation Equilibria of Meso-Tetrakis(4-carboxyphenyl)porphyrin with Viologens: Evidence for 1:1 and 1:2 Complexes and Induced Porphyrin Dimerization. *J. Phys. Chem. A* **2002**, *106*, 3235–3242.
65. Borisenko, V. E.; Gaponenko, S. V.; Gurin, V. S. *Physics, Chemistry, and Applications of Nanostructures*; Imperial College Press: London, UK, 2003.
66. Ourednik, J.; Ourednik, V.; Lynch, W. P.; Schachner, M.; Snyder, E. Y. Neural Stem Cells Display an Inherent Mechanism for Rescuing Dysfunctional Neurons. *Nat. Biotechnol.* **2002**, *20*, 1103–1110.
67. Riemer, J.; Hoepken, H. H.; Czerwinska, H.; Robinson, S. R.; Dringen, R. Colorimetric Ferrozine-Based Assay for the Quantitation of Iron in Cultured Cells. *Anal. Biochem.* **2004**, *331*, 370–375.
68. Shevchenko, A.; Wilm, M.; Vorm, O.; Mann, M. Mass Spectrometric Sequencing of Proteins Silver-Stained Polyacrylamide Gels. *Anal. Chem.* **1996**, *68*, 850–858.